

## Electronic Supplementary Information

### Alkyl-templated cocrystallization of long-chain bromoalkanes by lipid-like ionic liquids

Muhammadiqboli Musozoda,<sup>a</sup> Joseph Muller II,<sup>b</sup> Grace I. Anderson,<sup>b</sup> Mairead Boucher,<sup>c</sup> Matthias Zeller,<sup>d</sup> Casey C. Raymond,<sup>a</sup> Patrick C. Hillesheim,<sup>\*c</sup> Arsalan Mirjafari<sup>\*a</sup>

<sup>a</sup>Department of Chemistry, State University of New York at Oswego, New York 13126, United States

<sup>b</sup>Department Chemistry and Physics, Florida Gulf Coast University, Fort Myers, Florida 33913, United States

<sup>c</sup>Department Chemistry and Physics, Ave Maria University, Ave Maria, Florida 34142, United States

<sup>d</sup>Department of Chemistry, Purdue University, West Lafayette, Indiana 47907, United States

#### Corresponding authors:

E-mail: [arsalan.mirjafari@oswego.edu](mailto:arsalan.mirjafari@oswego.edu)

E-mail: [patrick.hillesheim@avemaria.edu](mailto:patrick.hillesheim@avemaria.edu)

## Experimental Procedures

**Materials and Instrumentation.** All commercial chemicals were used as received unless otherwise noted.  $^1\text{H}$ ,  $^{13}\text{C}$  and  $^{19}\text{F}$  NMR were performed on a JEOL 400 MHz NMR at 295 K. Chemical shifts ( $\delta$ ) are quoted in parts per million (ppm) and referenced to the appropriate NMR solvent residual peaks. ESI-MS analyses were performed by flow-injection on a Thermo Scientific ion trap mass spectrometer using HPLC grade acetonitrile and data were collected in positive and negative ion mode. SC-XRD experiments were carried out with Mo or Cu- $\text{K}\alpha$  radiation using Bruker AXS D8 Quest diffractometer with PhotonII or PhotonIII-C14 charge-integrating pixel array detectors (CPAD).

**Differential Scanning Calorimetry.** Melting points were measured using a TA Discovery 250 DSC Differential Scanning Calorimeter, calibrated using indium (melting point) and sapphire (heat capacity) references with a heating and subsequent cooling rate of 5  $^\circ\text{C}/\text{min}$ . Samples (5–10 mg) were loaded into DSC aluminium pans and heated to 150  $^\circ\text{C}$  for 5 min to remove any water absorbed from the environment. The samples were then cooled to  $-50$   $^\circ\text{C}$  and heated at a ramp rate of 5  $^\circ\text{C}/\text{min}$  to 150  $^\circ\text{C}$ . Their glass transition temperatures are reported offset of phase transitions as calculated by the TRIOS analysis software. To prevent concerns related to the volatility of bromoalkanes, the DSC analysis was conducted in a sealed system. Ten scans were carried out to identify the correct phase transitions by observing three overlapping cycles. All measurements were carried out under a nitrogen atmosphere and were reproducible to within  $\pm 1^\circ\text{C}$ , although varying the thermal history of the sample produced variations in the transition temperatures, a phenomenon often observed in ionic liquids.

**Synthetic Procedure.** Generally, the ILs with saturated side chains were synthesized using a reported procedure from the literature.<sup>1</sup> Briefly, 1 equiv. of 2-mercaptothiazole/2-mercapto-2-thiazoline and 1 equiv. of palmityl bromide/stearyl bromide were dissolved in  $\text{CH}_3\text{CN}$ . The mixture was vigorously stirred and refluxed overnight. The solvent was removed *in vacuo* yielding IL products of **3** and **4** as white solids in quantitative yields. The crude product was recrystallized from hot  $\text{CH}_3\text{CN}$ . The precipitate was separated *via* vacuum filtration through a sintered glass Büchner funnel and filter cakes were washed with cold  $\text{CH}_3\text{CN}$ . The compounds **3-16:0** and **3-18:0** were obtained as white solids in 92%-94% yield.  $^1\text{H}$  and  $^{13}\text{C}$  NMR were consistent with the structures. To improve the hydrolytic stability of compounds **4** for NMR studies, the bromide salts were converted to their bistriflimide analogues with these anions through anion metathesis reaction. IL **3-18:1** with iodide as the anion was synthesized using a procedure from our previous publication.<sup>2</sup>

**3-16:0.**  $^1\text{H}$  NMR (400 MHz,  $\text{CDCl}_3$ )  $\delta_{\text{H}}$  7.95 (d,  $J = 4.3$  Hz, 1H), 7.48 (d,  $J = 4.2$  Hz, 1H), 3.52 (t, 2H), 1.88-1.82 (m, 2H), 1.53-1.25 (m, 26H), 0.87 (t,  $J = 4.8$  Hz, 3H);  $^{13}\text{C}$  NMR (101 MHz,  $\text{CDCl}_3$ )  $\delta_{\text{C}}$  135.9, 119.4, 36.8, 32.0, 29.8, 29.7, 29.6, 29.5, 29.4, 29.0, 28.7, 28.1, 22.8, 14.2; MS (ESI):  $m/z$  342.5 ( $M = \text{C}_{19}\text{H}_{36}\text{NS}_2^+$ , calcd. 342.2).

**3-18:0.**  $^1\text{H}$  NMR (400 MHz,  $\text{CDCl}_3$ )  $\delta_{\text{H}}$  7.98 (d,  $J = 3.9$  Hz, 1H), 7.51 (d,  $J = 4.1$  Hz, 1H), 3.48-3.31 (m, 2H), 2.70-2.16 (m, 2H), 2.03-1.80 (m, 2H), 1.52-1.24 (m, 30H), 0.86 (t,  $J = 6.9$  Hz, 3H);  $^{13}\text{C}$  NMR (101 MHz,  $\text{CDCl}_3$ )  $\delta_{\text{C}}$  135.9, 119.4, 36.8, 32.0, 29.8, 29.7, 29.6, 29.5, 29.4, 29.0, 28.7, 28.1, 22.8, 14.2; MS (ESI):  $m/z$  370.1 ( $M = \text{C}_{21}\text{H}_{40}\text{NS}_2^+$ , calcd. 370.3).

**3-18:1.**  $^1\text{H}$  NMR (400 MHz,  $\text{DMSO}-d_6$ )  $\delta_{\text{H}}$  7.70-7.62 (m, 2H), 5.30 (t,  $J = 4.7$  Hz, 2H), 3.17 (t,  $J = 7.2$  Hz, 2H), 1.95 (t,  $J = 6.1$  Hz, 4H), 1.65 (q,  $J = 7.5$  Hz, 2H), 1.37-1.22 (m, 24H), 0.84-0.81 (m, 3H);  $^{13}\text{C}$  NMR (101 MHz,  $\text{DMSO}-d_6$ )  $\delta_{\text{C}}$  164.0, 142.7, 129.7, 120.0, 33.6, 31.3, 29.1, 29.1, 28.9, 28.7, 28.6, 28.5, 28.5, 28.0, 26.6, 22.1, 14.0; MS (ESI):  $m/z$  368.8 ( $M = \text{C}_{21}\text{H}_{38}\text{NS}_2^+$ , calcd. 368.3).

**4-16:0.**  $^1\text{H}$  NMR (400 MHz,  $\text{CDCl}_3$ )  $\delta_{\text{H}}$  4.44 (t,  $J = 8.6$  Hz, 1H), 3.76 (t,  $J = 8.6$  Hz, 1H), 3.41-3.27 (m, 2H), 1.87-1.74 (m, 2H), 1.44-1.37 (m, 2H), 1.33-1.24 (m, 24H), 0.86 (t,  $J = 6.9$  Hz, 3H);  $^{13}\text{C}$  NMR (101 MHz,  $\text{CDCl}_3$ )  $\delta_{\text{C}}$  193.2, 124.5, 121.3, 118.1, 117.2, 114.9, 77.7, 77.4, 77.3, 77.1, 76.8, 55.2, 36.2, 34.2, 33.0, 32.9, 32.0, 29.8, 29.7, 29.7, 29.6, 29.6, 29.5, 29.5, 29.4, 29.2, 28.9, 28.9, 28.5, 28.3, 24.8, 22.8, 14.2; MS (ESI):  $m/z$  344.9 ( $M = \text{C}_{19}\text{H}_{38}\text{NS}_2^+$ , calcd. 344.2).

**4-18:0.**  $^1\text{H}$  NMR (400 MHz,  $\text{CDCl}_3$ )  $\delta_{\text{H}}$  7.98 4.44 (t,  $J = 8.5$  Hz, 2H), 3.78 (t,  $J = 8.6$  Hz, 2H), 3.29 (t,  $J = 7.3$  Hz, 2H), 1.79 (t,  $J = 7.5$  Hz, 2H), 1.43 (t,  $J = 7.5$  Hz, 2H), 1.32-1.24 (m, 30H), 0.86 (t,  $J = 6.7$  Hz, 3H);  $^{13}\text{C}$  NMR (101 MHz,  $\text{CDCl}_3$ )  $\delta_{\text{C}}$  194.2, 124.5, 121.3, 118.1, 114.9, 77.4, 77.3, 77.1, 76.8, 54.9, 36.3, 34.1, 32.9, 32.0, 30.1, 29.8, 29.7, 29.6, 29.5, 29.4, 29.2, 28.9, 28.4, 28.2, 24.8, 22.8, 14.2; MS (ESI):  $m/z$  372.3 ( $M = \text{C}_{21}\text{H}_{42}\text{NS}_2^+$ , calcd. 372.7).

**3-16:0/palmityl bromide.**  $^1\text{H}$  NMR (400 MHz,  $\text{CDCl}_3$ )  $\delta_{\text{H}}$  7.94 (d,  $J = 2.1$  Hz, 1H), 7.50 (d,  $J = 1.8$  Hz, 1H), 3.55-3.33 (m, 4H), 1.91-1.76 (m, 4H), 1.40 (s, 3H), 1.36-1.16 (49H), 0.86 (dd,  $J = 7.1, 4.8$  Hz, 6H);  $^{13}\text{C}$  NMR (101 MHz,  $\text{CDCl}_3$ )  $\delta_{\text{C}}$  134.7, 118.9, 37.2, 32.0, 27.8, 26.3, 20.0, 12.2.

**3-18:0/stearyl bromide.**  $^1\text{H}$  NMR (400 MHz,  $\text{CDCl}_3$ )  $\delta_{\text{H}}$  7.91 (d,  $J = 2.1$  Hz, 1H), 7.50 (d,  $J = 1.8$  Hz, 1H), 3.45-3.38 (m, 4H), 1.99-1.83 (m, 4H), 1.47 (s, 11H), 1.36-1.16 (93H), 0.86 (dd,  $J = 7.1, 4.8$  Hz, 9H);  $^{13}\text{C}$  NMR (101 MHz,  $\text{CDCl}_3$ )  $\delta_{\text{C}}$  133.4, 117.5, 114.4, 35.1, 30.9, 30.2 29.7, 29.5, 29.4, 29.0, 28.6, 28.3, 22.7, 14.2.

**X-ray crystallographic data.** For the SC-XRD studies, equimolar mixtures of ILs **3-16:0** and **3-18:0** were prepared along with their corresponding 1-bromoalkanes. The recrystallization process was carried out through solvent evaporation at room temperature. ~20 mg of the IL/RBr compounds were dissolved in acetonitrile (4.5 mL) and methanol (0.5 mL), maintaining a

9:1 ratio, within a 25 mL round-bottom flask. The round-bottom flask was placed in a  $-20\text{ }^{\circ}\text{C}$  freezer for 24 hours before the crystallization process commenced. Sample crystallized at room temperature after 6-10 weeks.

We aim to enhance the clarity of the crystallization process within this system. The current presentation of the system demonstrates a reproducible crystallization of a mixture of the ionic liquid and alkyl bromide, resulting in a heterogeneous mixture of the following crystalline samples: the cocrystal (IL + alkyl bromide), the IL, and the alkyl bromide. When an aliquot of a mixture of the IL and the alkyl bromide is set for crystallization, a combination of these three crystalline phases forms. We were unable to collect detailed, reliable Powder XRD data for our samples due to their low melting points coupled with the hygroscopic nature of the ionic liquids. The high-intensity X-ray radiation in the diffractometer caused the samples to melt in less than 2 minutes. However, we have confirmed the presence of crystalline samples through repeated crystal growths and by comparing the unit cells of the new crystals with those reported in Table S1.

**Table S1.** Unit cell parameters of repeated crystal samples.

	Sample 1		Sample 2		Sample 3	
	<i>a, b, c</i> (Å)	$\alpha, \beta, \gamma$ ( $^{\circ}$ )	<i>a, b, c</i> (Å)	$\alpha, \beta, \gamma$ ( $^{\circ}$ )	<i>a, b, c</i> (Å)	$\alpha, \beta, \gamma$ ( $^{\circ}$ )
3-18:0	8.6976 (6), 9.0477 (6), 15.3351 (11)	96.503 (3), 101.075 (3), 100.606 (3)	8.6836 (5), 9.0510 (5), 15.3318 (8)	96.133 (5), 101.724 (5), 100.965 (3)	8.6861(7), 9.0440 (2), 15.3221 (2)	96.290 (9), 100.799 (4), 100.775 (6)
3-16:0/C <sub>16</sub> Br	8.7215 (5), 9.0562 (6), 25.5173 (16)	93.301 (2), 91.998 (2), 106.020 (2)	8.2418 (7), 9.2158 (6), 25.3245 (11)	93.256 (3), 92.001 (3), 106.090 (5)	8.8524 (5), 9.0698 (5), 25.6530 (9)	93.657 (2), 91.785 (4), 106.100 (3)
C <sub>18</sub> Br	5.561 (3), 7.204 (3), 46.69 (3)	87.22 (3), 87.14 (3), 89.974 (19)	5.1248 (4), 7.132 (5), 46.87 (7)	87.11 (7), 87.19 (5), 89.899 (11)		

The formation of this mixture of crystals follows the logic discussed in the main narrative of the work. The primary driving force for the formation of these crystalline samples is the maximization of alkyl-alkyl interactions (along with the coulombic interactions for the ILs). All three crystalline samples the co-crystals exhibit similar alkyl-alkyl interactions, making these interactions interchangeable concerning crystal formation. The formation of chalcogen bonds in the cocrystal. Therefore, it helps stabilizing the formation of this particular crystal, although the exact energetic contribution of these interactions to the lattice stabilization energy is unknown. We are currently working on computational modelling to determine these values. It follows that increasing the energetic contribution of these  $\sigma$ -hole interactions to the overall stabilization of the cocrystal system would enhance the propensity for the formation of the cocrystal compared to the other two crystals. Increasing the electropositive region of the sulfur moiety on the cation through electronic modification of the heterocycle by adding electron-withdrawing groups would help increase the contribution of these  $\sigma$ -hole interactions. Synthetic modification of the cations is an approach we are pursuing for our follow-up work on these compounds.

Single crystal data of the samples were collected on a Bruker Quest diffractometer with kappa geometry, a Cu  $\square$  wavelength ( $\lambda = 1.54178\text{ \AA}$ ) I- $\mu$ -S microsource X-ray tube, laterally graded multilayer (Goebel) mirror single crystal for monochromatization, a Photon II or Photon III-C14 area detector and an Oxford Cryosystems low temperature device. Examination and data collection were performed at 150 K. Data was collected, reflections were indexed and processed, and the files scaled and corrected for absorption using SADABS<sup>3</sup> and APEX3 or APEX4.<sup>4</sup> The space groups were assigned using XPREP within the SHELXTL suite of programs,<sup>5,6</sup> the structures were solved by dual methods using ShelXT<sup>6</sup> and refined by full matrix least squares against  $F^2$  with all reflections with Shelxl2018 or Shelxl2019<sup>7</sup> using the graphical interface ShelXle.<sup>8</sup> H atoms were positioned geometrically and constrained to ride on their parent atoms. C–H bond distances were constrained to 0.95 Å for alkene C–H moieties, and to 0.99 and 0.98 Å for aliphatic CH<sub>2</sub> and CH<sub>3</sub> moieties, respectively. Methyl H atoms were allowed to rotate but not to tip to best fit the experimental electron density. N–H bond lengths were constrained to 0.88 Å.  $U_{iso}(\text{H})$  values were set to a multiple of  $U_{eq}(\text{C/N})$  with 1.5 for CH<sub>3</sub> and 1.2 for N–H, C–H and CH<sub>2</sub> units, respectively.  $U_{ij}$  components of ADPs of O and Cl atoms sharing the same site were constrained to be identical.

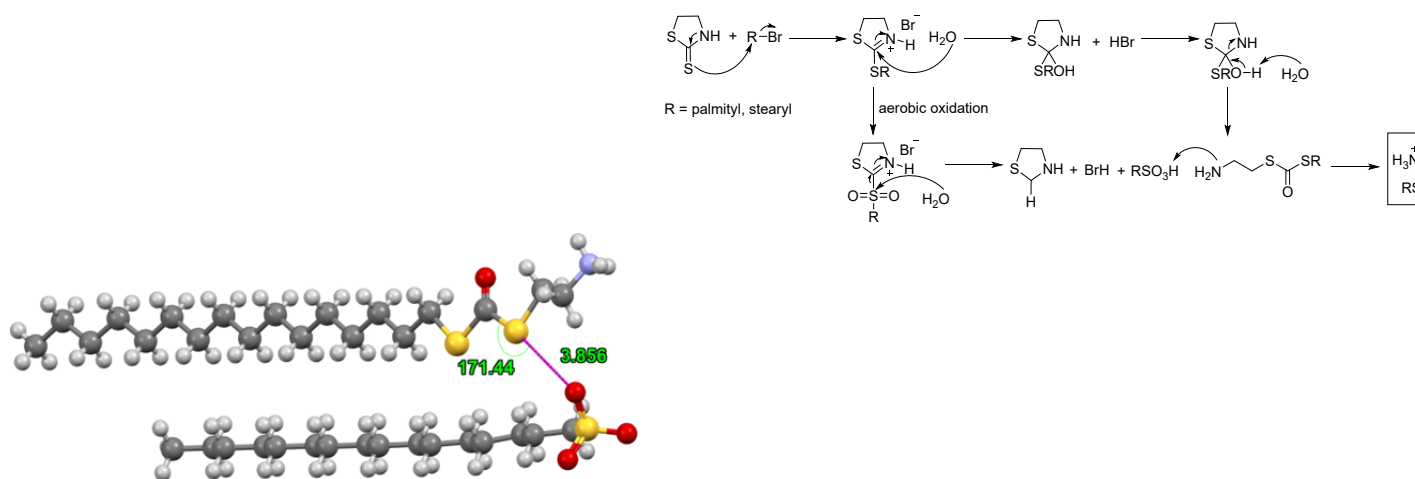
For the structure of **IL 3-16\_C16Br** the terminal methyl group and the bromide atom of the alkyl amide are disordered with each other. The CH<sub>2</sub>–CH<sub>3</sub> distances of disordered fragments were restrained to 1.53(2) Ångstrom.  $U_{ij}$  components of ADPs for disordered atoms closer to each other than 2.0 Å were restrained to be similar. The ADPs of atoms Br2 and C35B were constrained to be identical. Subject to these conditions the occupancy ratio was refined to 0.7977(18) to 0.2023(18).

Data quality for **stearyl bromide** was low due to crystal size (flake like very thin crystals). The structure was refined as a 2-component twin. Inspection of the diffraction pattern showed no distinguishable twin moieties. Thus, only pseudo-merohedral twinning was considered, with twin transformation matrices as suggested via the program Rotax.<sup>9</sup> Multiple twin transformations were tested, individually and in combination (using the program 2twin<sup>10</sup>). Best results were obtained using a 180° rotation around the reciprocal direction (0 2 1), transformation matrix -1 0 0 0 1 0 0 1 -1. The twin ratio refined to 0.759(6) to 0.241(6).

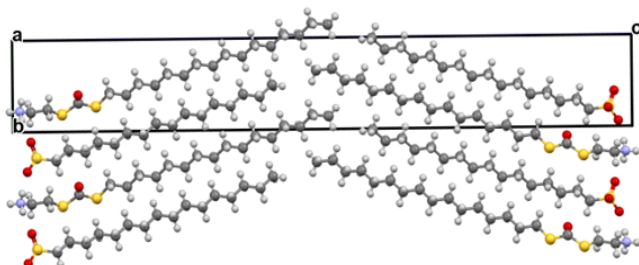
Complete crystallographic data, in CIF format, were deposited with the Cambridge Crystallographic Data Centre. CCDC numbers 2294544, 2294545, 2294546, and 2294547 contain the supplementary crystallographic data for this paper. These data can be obtained free of charge from The Cambridge Crystallographic Data Centre via [www.ccdc.cam.ac.uk/data\\_request/cif](http://www.ccdc.cam.ac.uk/data_request/cif).

Hirshfeld surfaces, their corresponding images, and fingerprint plots were calculated using the program *CrystalExplorer21*.<sup>11</sup> Other images and bond distances were analyzed using Olex2<sup>12</sup> and Mercury.<sup>13</sup>

**Crystallographic data of the hydrolyzed structure of 4-16:0.** The hydrolyzed structure of 4-16:0 provides further evidence as to the underlying cooperative interactions leading to crystal growth (Figure S1). As observed in the packing diagram of the hydrolyzed structure (Figure S2), clearly defined regions are formed wherein the hydrophobic alkyl tails are aligned, maximizing H...H interactions. Concomitantly, the hydrophilic moieties form an extended planar network linked through multiple hydrogen interactions. When contrasted with the cocrystal's planar the ring, the ammonium ion's tetrahedral geometry leads to the formation of a more complex network of H-bonds as all three of the N—H moieties interact with adjacent sulfates. This leads to the formation of "R" \_ "4" ^ "4" (12) and "R" \_ "6" ^ "6" (18) H-bonding motifs when considering all the individual N—H moieties (Figure S3).

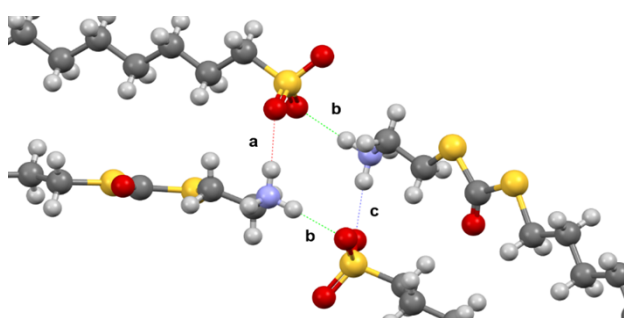


**Figure S1.** The plausible mechanism of hydrolysis of 4-16:0 (top) and asymmetric unit of the structure of the hydrolyzed product shown with 50% probability ellipsoids (bottom). The chalcogen bond within the crystal is shown in pink dotted line. Distances are shown in Å.



**Figure S2.** Packing diagram of hydrolyzed crystal of 4-16:0 viewed down the crystallographic A axis.

Remarkably, the sulfur atoms within the cationic moiety display chalcogen bonding interactions with symmetry adjacent sulfate molecules (Figure S1). Specifically, S2 is interacting with O1 at a distance of 3.856(4) Å with an angle of 171° ( $d(S1 \cdots O2i)$ ,  $\angle C19-S2 \cdots O1i$ ,  $i = +x, 1+y, +z$ ). This distance and angle are within the expected ranges for these interactions. Of note, however, is that only S2 displays chalcogen bonding interactions with the other sulfur showing close contact with adjacent hydrogen atoms. Thus, within this serendipitous crystalline solid formed from the neat IL, H-bonding and  $\sigma$ -hole interactions similar to those seen within the cocrystal point to the complementary manner in which these interactions contribute to the formation of the extended structure of these lipid-like ionic liquids.



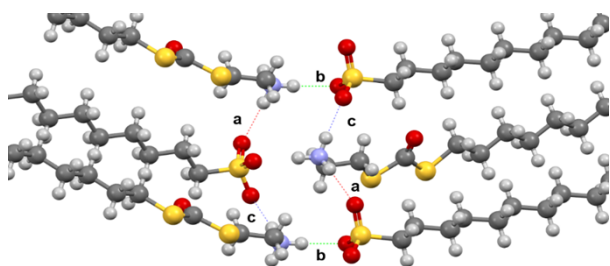


**Figure S3.** Depiction of the  $R_4^4(12)$  H-bonding ring (top) and the  $R_6^6(18)$  ring (bottom). Portions of the alkyl chains are omitted for clarity.

Several relevant details can be gleaned by contrasting the cocrystal and the hydrolyzed structure **4-16:0**. First, following the discussion of hydrogen and chalcogen bonds, a similar planar arrangement can be observed within both compounds when following these interactions (Figure S4). The organization of the two crystals is similar as strong H-bonds and H $\cdots$ H interactions link the components of the crystal while chalcogen bonds act as supplementary interactions, helping to stabilize the components.

Second, we note the importance of the H-bonding within the hydrophilic portion. Examining a single cation-anion pair within the hydrolyzed structure of **4-16:0**, we observe that the moieties arrange to preferentially allow for the formation of H-bonding as opposed to formation of the chalcogen bonds. In brief, the sulfate moiety can form both H-bonds and chalcogen bonds. However, the positioning is such that the most H-bonds can be formed. This observation points to the importance of H-bonding in acting as a guiding supramolecular motif for the construction of the cocrystal system. Despite this, the presence of a chalcogen bond within the hydrolyzed system appears more than coincidental given the geometries observed.

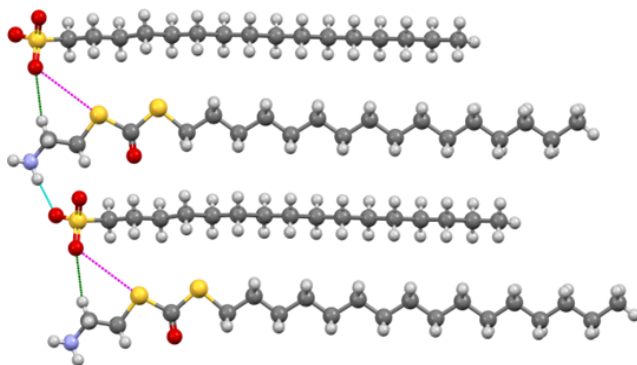


**Figure S4.** Depiction of the hydrogen bonding and chalcogen bonding forming a plane within the crystal. Chalcogen bonding is shown in pink, N—H $\cdots$ O hydrogen bond in light blue, and C—H $\cdots$ O H-bonding in dark green.

Finally, no interdigitation of the alkyl chains is observed within the hydrolyzed structures of **4-16:0** in contrast to that observed within **3-18:0**, wherein the alkyl chains on the cation are interdigitated. Speculatively, this is due to the ammonium cation forming a more complex, tetrahedral hydrogen bonding network. In contrast, the planar N—H H-bonding within **3-16:0** only allows for a single H-bond to form in one direction. Thus, given the geometric requirements of a H-bond, this demonstrates how the H-bonding within the cocrystal is a vital part of developing the arrangement of the alkyl template, allowing for the incorporation of the alkyl halide within the cocrystal.

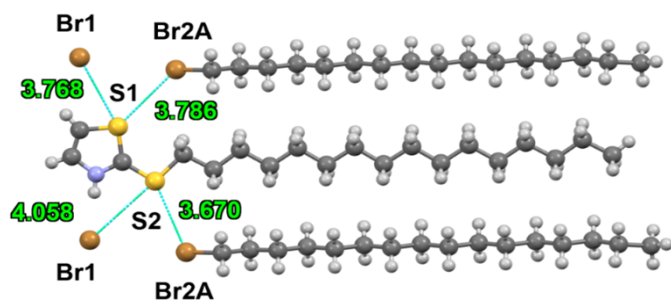


**Figure S5.** Chalcogen bonds in **3-16:0** (blue lines). Distances are shown in green in Å.

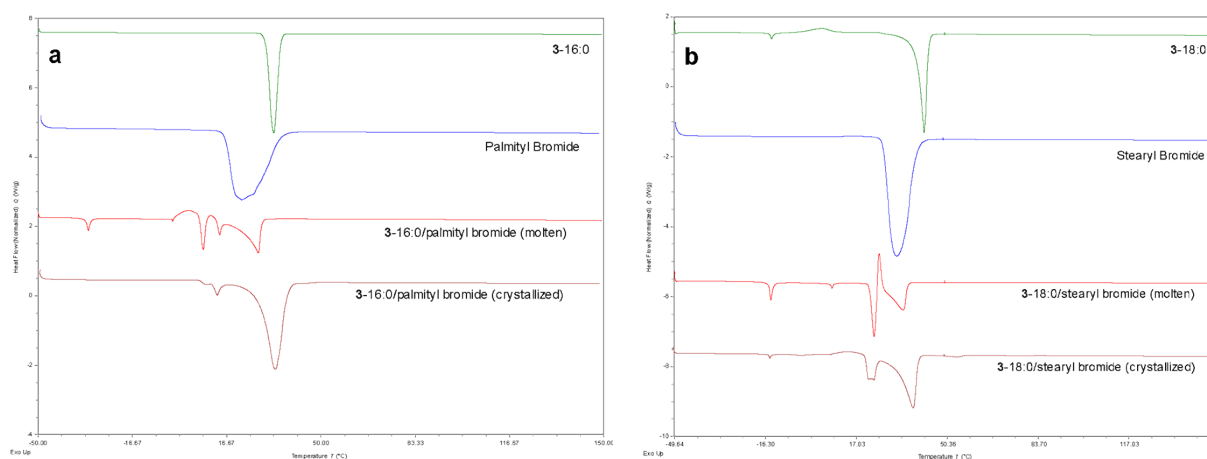


**Figure S6.** Comparison of notable phase behaviours for (a): **3-16:0**, 1-bromohexadecane, and **3-16:0/1-bromohexadecane** (molten and crystallized) (b): **3-18:0**, 1-bromooctadecane, and **3-18:0/1-bromooctadecane** (molten and crystallized). The DSC thermograms' y-scales were offset for clarity but not rescaled.

**Table S2.** Phase transitions including melting points of the IL-bromoalkane complexes.<sup>a</sup>

Compounds	$T_m$ (°C)
<b>3-16:0</b>	$30.68 \pm 0.2$
<b>3-18:0</b>	$39.30 \pm 0.1$
Palmityl bromide	$16.24 \pm 0.1$
Stearyl bromide	$26.92 \pm 0.1$
<b>3-16:0/palmityl bromide (molten)</b>	$13.01 \pm 0.2, 22.23 \pm 0.3$
<b>3-18:0/stearyl bromide (molten)</b>	$21.36 \pm 0.3, 25.61 \pm 0.3$
<b>3-16:0/palmityl bromide (crystallized)</b>	$11.73 \pm 0.3, 28.50 \pm 0.2$
<b>3-18:0/stearyl bromide (crystallized)</b>	$20.29 \pm 0.3, 31.99 \pm 0.4$

<sup>a</sup> Measurements were taken in open pans under N<sub>2</sub> gas at a ramp rate of 5 °C/min

**Table S3.** Crystal data of reported crystals in this work.

	IL 3-18	IL 3-16_C16Br
<b>Crystal Data</b>		
Chemical formula	C <sub>21</sub> H <sub>40</sub> NS <sub>2</sub> ·Br	Br·C <sub>16</sub> H <sub>33</sub> Br·C <sub>19</sub> H <sub>36</sub> NS <sub>2</sub>
<i>M<sub>r</sub></i>	450.57	727.85
Crystal system, space group	Triclinic, <i>P</i> <sub>1</sub>	Triclinic, <i>P</i> <sub>1</sub>
Temperature (K)	150	150
<i>a</i> , <i>b</i> , <i>c</i> (Å)	8.6976 (6), 9.0477 (6), 15.3351 (11)	8.7215 (5), 9.0562 (6), 25.5173 (16)
$\alpha$ , $\beta$ , $\gamma$ (°)	96.503 (3), 101.075 (3), 100.606 (3)	93.301 (2), 91.998 (2), 106.020 (2)
<i>V</i> (Å <sup>3</sup> )	1150.16 (14)	1931.3 (2)
<i>Z</i>	2	2
Radiation type	Cu <i>K</i> $\alpha$	Cu <i>K</i> $\alpha$
$\mu$ (mm <sup>-1</sup> )	4.14	3.82
Crystal size (mm)	0.40 × 0.20 × 0.06	0.4 × 0.32 × 0.05
<b>Data Collection</b>		
Diffractometer	Bruker AXS D8 Quest diffractometer with PhotonIII_C14 charge-integrating and photon counting pixel array detector	Bruker AXS D8 Quest diffractometer with PhotonII charge-integrating pixel array detector
Absorption correction	Multi-scan, SADABS 2016/2: Krause, L., Herbst-Irmer, R., Sheldrick G.M. & Stalke D., J. Appl. Cryst. 48 (2015) 3-10.	
<i>T</i> <sub>min</sub> , <i>T</i> <sub>max</sub>	0.491, 0.754	0.465, 0.754
No. of measured, independent and observed [ <i>I</i> > 2 $\sigma$ ( <i>I</i> )] reflections	20356, 4917, 4190	22819, 7739, 6982
<i>R</i> <sub>int</sub>	0.072	0.066
(sin $\theta$ / $\lambda$ ) <sub>max</sub> (Å <sup>-1</sup> )	0.638	0.640
<b>Refinement</b>		
<i>R</i> [ <i>F</i> <sup>2</sup> > 2 $\sigma$ ( <i>F</i> <sup>2</sup> )], <i>wR</i> ( <i>F</i> <sup>2</sup> ), <i>S</i>	0.043, 0.121, 1.13	0.049, 0.128, 1.07
No. of reflections	4917	7739
No. of parameters	227	377
No. of restraints	-	38
H-atom treatment	H-atom parameters constrained.	

$\Delta\rho_{\max}, \Delta\rho_{\min}$ (e $\text{\AA}^{-3}$ )	0.49, -1.04	0.67, -0.49
Absolute structure	-	-
Absolute structure parameter	-	-

**Table S3** (continued). Crystal data of reported crystals in this work.

	<b>IL 4-16-hydrolyzed</b>	<b>Stearyl bromide</b>
<b>Crystal Data</b>		
Chemical formula	$\text{C}_{19}\text{H}_{40}\text{NOS}_2 \cdot \text{C}_{16}\text{H}_{33}\text{O}_3\text{S}$	$\text{C}_{18}\text{H}_{37}\text{Br}$
$M_r$	668.12	333.38
Crystal system, space group	Monoclinic, $P2_1$	Triclinic, $P\bar{1}$
Temperature (K)	150	150
$a, b, c$ ( $\text{\AA}$ )	5.0644 (2), 7.3853 (3), 51.831 (2)	5.561 (3), 7.204 (3), 46.69 (3)
$\alpha, \beta, \gamma$ ( $^\circ$ )	90.179 (2)	87.22 (3), 87.14 (3), 89.974 (19)
$V$ ( $\text{\AA}^3$ )	1938.60 (14)	1865.9 (17)
$Z$	2	4
Radiation type	Cu $K\alpha$	Cu $K\alpha$
$\mu$ ( $\text{mm}^{-1}$ )	2.01	2.88
Crystal size (mm)	0.09 $\times$ 0.08 $\times$ 0.02	0.23 $\times$ 0.18 $\times$ 0.03
<b>Data Collection</b>		
Diffractometer	Bruker AXS D8 Quest diffractometer with PhotonIII_C14 charge-integrating and photon counting pixel array detector	
Absorption correction	Multi-scan, <i>SADABS</i> 2016/2: Krause, L., Herbst-Irmer, R., Sheldrick G.M. & Stalke D., <i>J. Appl. Cryst.</i> 48 (2015) 3-10.	
$T_{\min}, T_{\max}$	0.656, 0.754	0.1712, 0.3289
No. of measured, independent and observed [ $I > 2\sigma(I)$ ] reflections	24550, 7943, 6278	19045, 7606, 3909
$R_{\text{int}}$	0.063	0.098
$(\sin \theta/\lambda)_{\text{max}}$ ( $\text{\AA}^{-1}$ )	0.642	
<b>Refinement</b>		
$R[F^2 > 2\sigma(F^2)], wR(F^2), S$	0.057, 0.144, 1.03	0.122, 0.3586, 0.99
No. of reflections	7943	7606

No. of parameters	392	346
No. of restraints	1	0
H-atom treatment	H-atom parameters constrained.	
$\Delta\rho_{\max}, \Delta\rho_{\min}$ (e Å <sup>-3</sup> )	0.30, -0.26	2.15, -1.14
Absolute structure	Refined as an inversion twin.	-
Absolute structure parameter	0.13 (3)	-

## References

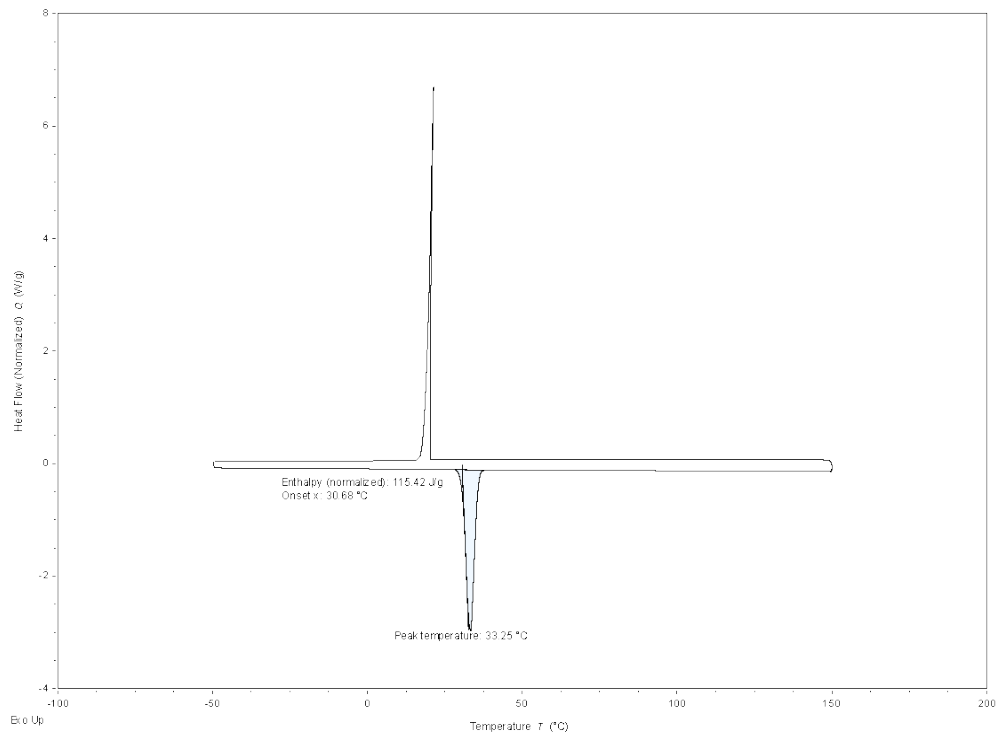
1. R. A. O'Brien, M. S. Zayas, S. T. Nestor, J. C. Gaitor, L. M. Paul, F. A. Edhegard, S. Minkowicz, R. E. Sykora, Y. Sheng, S. F. Michael, S. Isern, A. Mirjafari, *New J. Chem.* **2016**, *40*, 7795–7803.
2. R. A. O'Brien, P. C. Hillesheim, M. Soltani, K. J. Badilla-Nunez, B. Siu, M. Musozoda, K. N. West, J. H. Jr. Davis, A. Mirjafari, *J. Phys. Chem. B* **2023**, *127*, 1429–1442.
3. L. Krause, R. Herbst-Irmer, G. M. Sheldrick, D. Stalke, *J. Appl. Crystallogr.* **2015**, *48*, 3–10.
4. Bruker Apex3, Apex 4, SAINT; Bruker Advanced X-ray Solutions; Bruker AXS Inc: Madison, Wisconsin, USA, 2019.
5. SHELXTL Suite of Programs; Bruker Advanced X-ray Solutions; Bruker AXS Inc: Madison, Wisconsin, USA, 2000.
6. G. M. Sheldrick, *Acta Cryst.* **2015**, *A71*, 3–8
7. G. M. Sheldrick, *Acta Cryst.* **2015**, *C71*, 3–8.
8. C. B. Hübschle, G. M. Sheldrick, B. Dittrich, *J. Appl. Cryst.* **2011**, *44*, 1281–1284.
9. R. I. Cooper, R. O. Gould, S. Parsons, D. J. Watkin, *J. Appl. Cryst.* **2002**, *35*, 168–174.
10. A. M. Champsaur, J. Yu, X. Roy, D. W. Paley, M. L. Steigerwald, C. Nuckolls, C. M. Bejger, *ACS Cent. Sci.* **2017**, *3*, 1050–1055.
11. P. R. Spackman, M. J. Turner, J. J. McKinnon, S. K. Wolff, D. J. Grimwood, D. Jayatilaka, M. A. Spackman, *J. Appl. Cryst.* **2021**, *54*, 1006–1011.
12. O. V. Dolomanov, L. J. Bourhis, R. J. Gildea, J. A. K. Howard, H. Puschmann, *J. Appl. Crystallogr.* **2009**, *42*, 339–341.
13. C. F. Macrae, I. J. Bruno, J. A. Chisholm, P. R. Edgington, P. McCabe, E. Pidcock, L. Rodriguez-Monge, R. Taylor, J. van de Streek, P. A. Wood, *J. Appl. Cryst.* **2008**, *41*, 466–470.

## Author Contributions

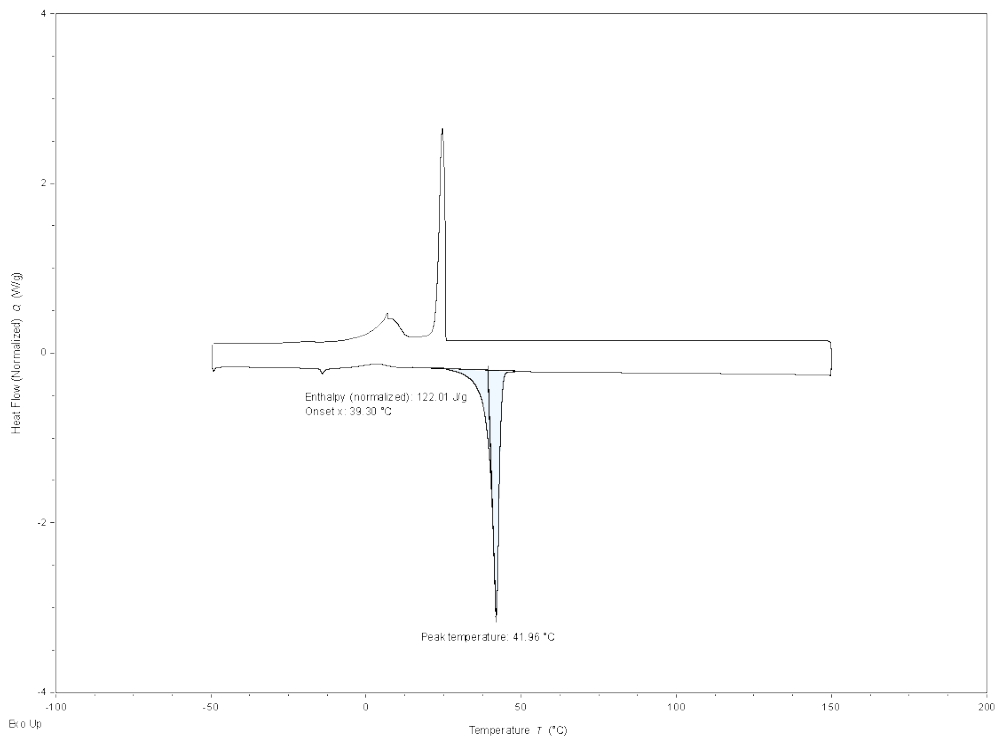
CRedit: Muhammadiqboli Musozoda formal analysis (lead), investigation (lead), methodology (lead), validation (supporting), writing-review & editing (supporting); Joseph Muller II formal analysis (lead), investigation (lead), methodology (lead), validation (supporting), writing-review & editing (supporting); Grace I. Anderson formal analysis (supporting), investigation (supporting), methodology (supporting), validation (lead), writing-review & editing (supporting); Christiane Carlos, formal analysis (supporting), investigation (supporting), methodology (supporting), validation (lead), writing-review & editing (supporting); Mairead Boucher formal analysis (supporting), investigation (supporting), methodology (supporting), validation (lead), writing-review & editing (supporting); Casey C. Raymond data curation (lead), investigation (supporting), writing-original draft (supporting), writing-review & editing (supporting); Patrick C. Hillesheim conceptualization (equal), data curation (equal), formal analysis (equal), investigation (equal), methodology (equal), writing-original draft (equal), writing review & editing (equal); Matthias Zeller formal analysis (supporting), investigation (supporting), funding acquisition (supporting), supervision (supporting), writing-original draft (lead), writing-review & editing (supporting); Arsalan Mirjafari conceptualization (lead), data curation (lead), funding acquisition (lead), supervision (lead), writing-original draft (lead), writing-review & editing (lead).

## DSC thermograms

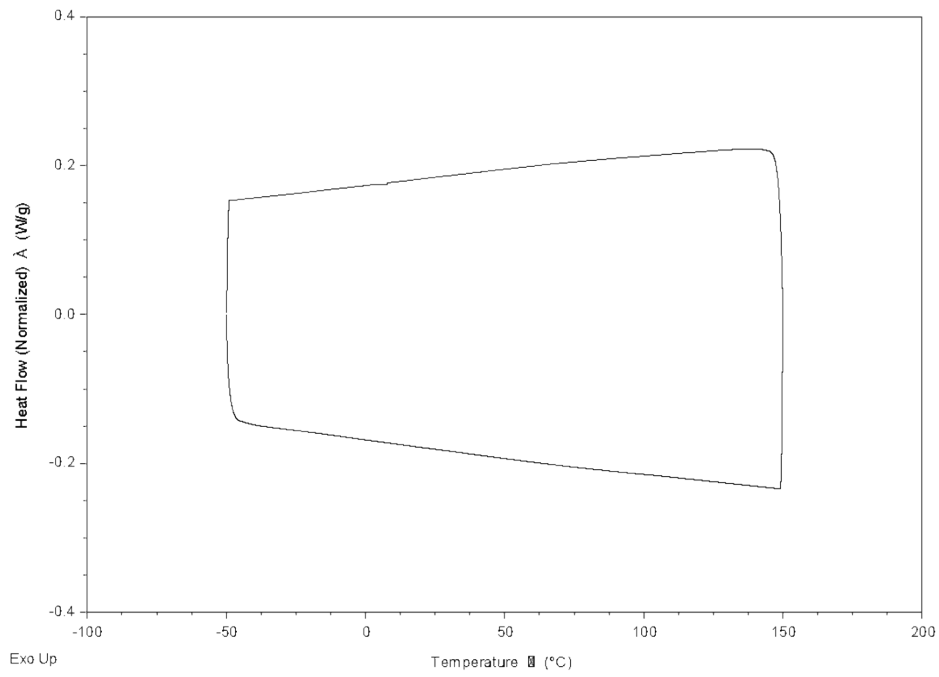
3-16:0



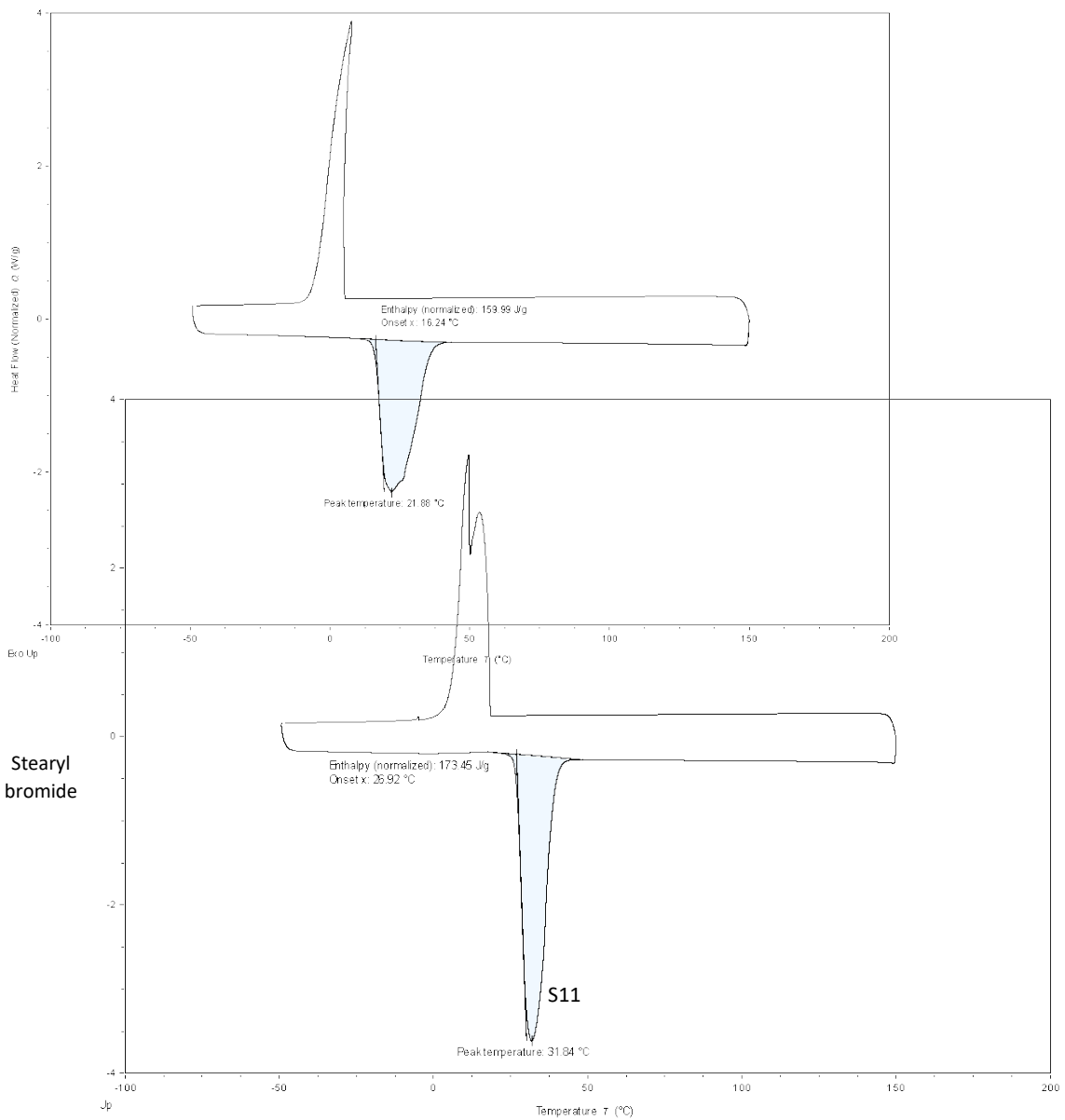
3-18:0



3-18:1

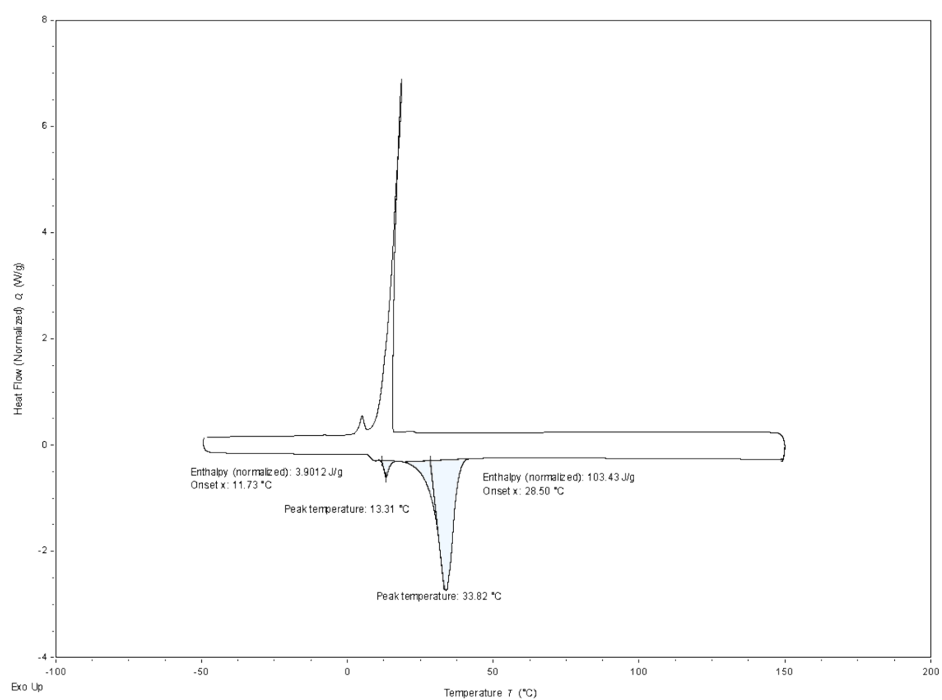


**Palmityl bromide**

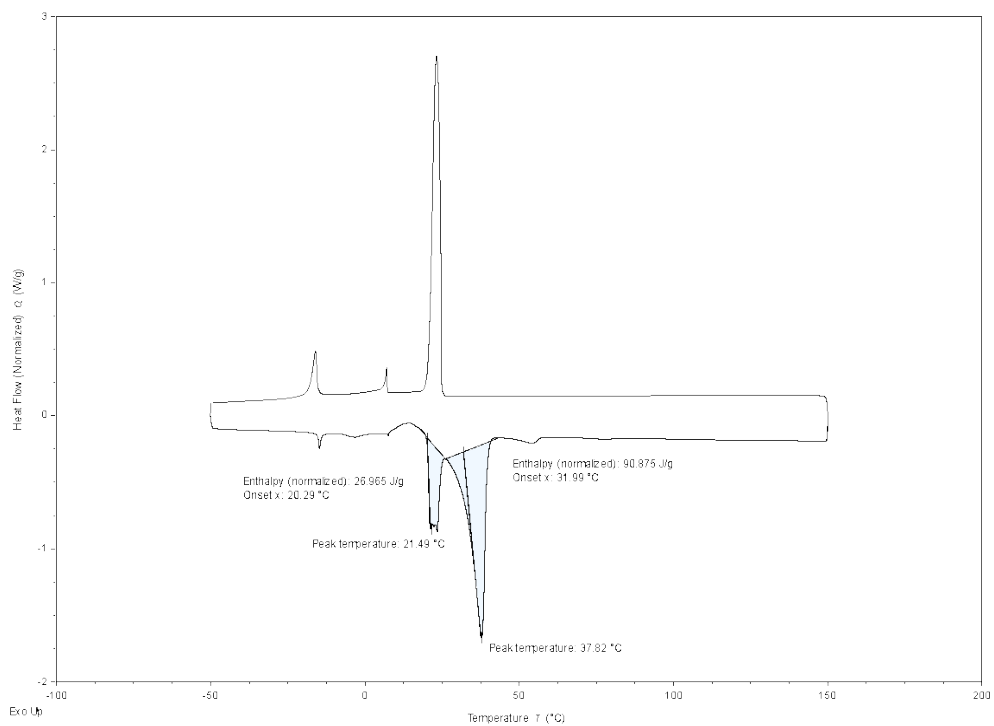


**Stearyl bromide**

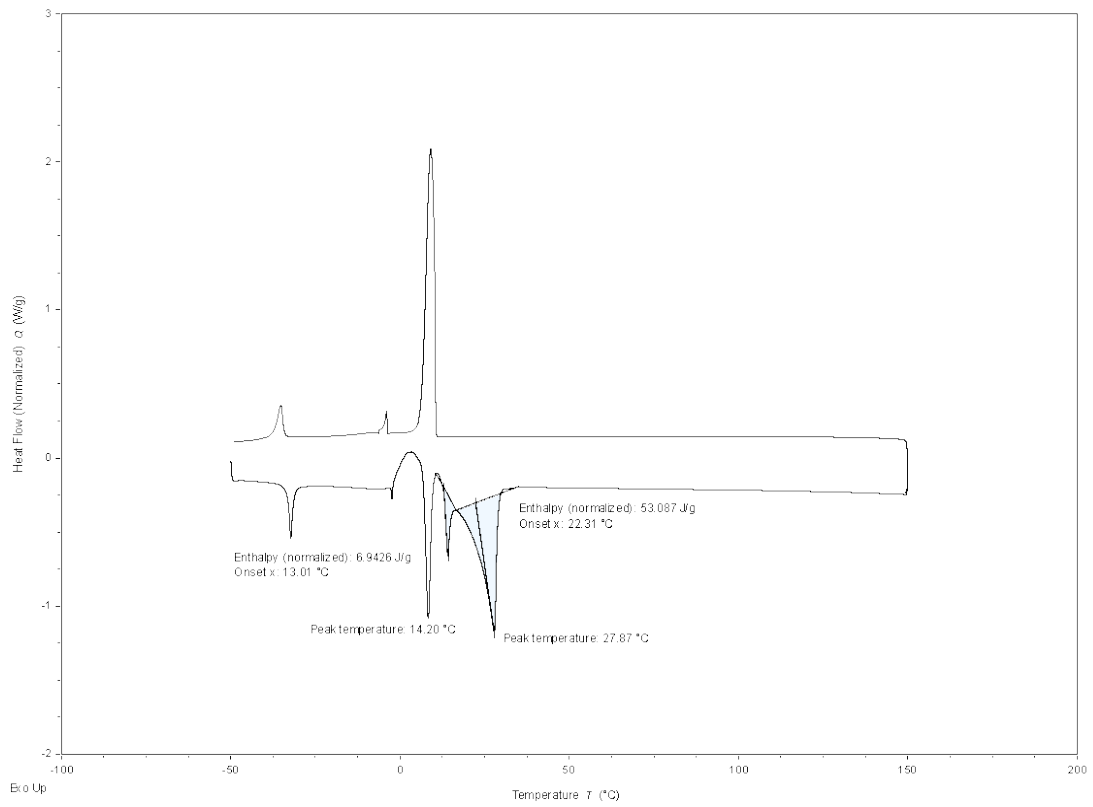
### 3-16:0/palmityl bromide (crystallized)



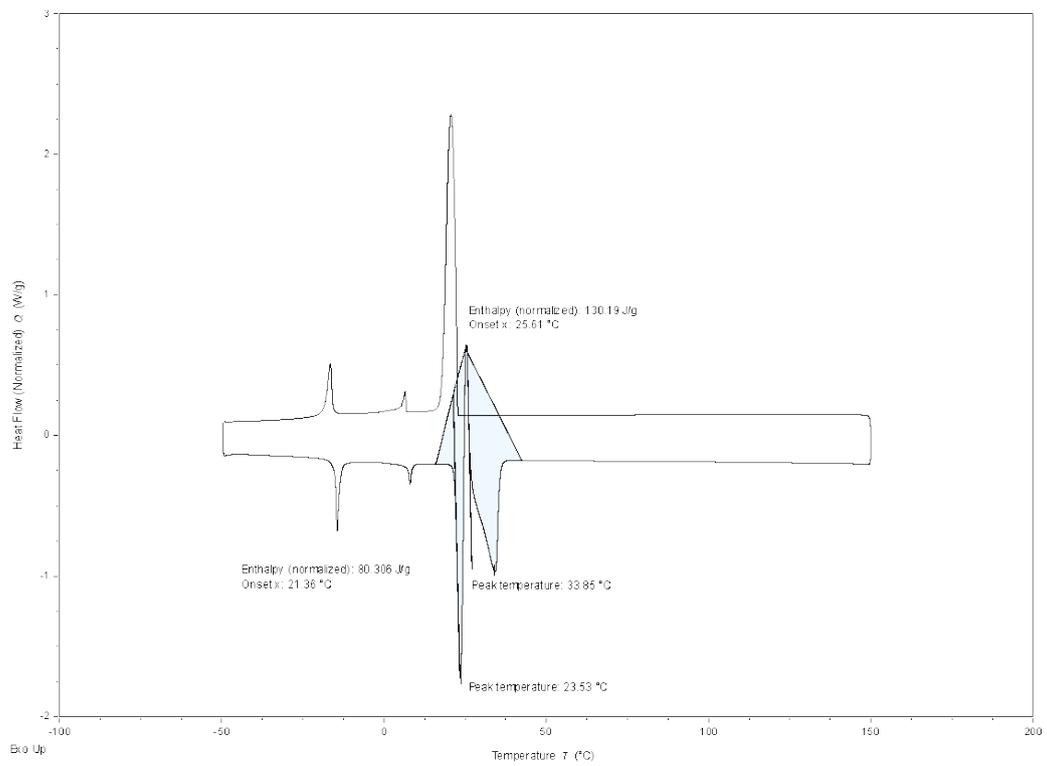
### 3-18:0/stearyl bromide (crystallized)



### 3-16:0/palmityl bromide (molten)



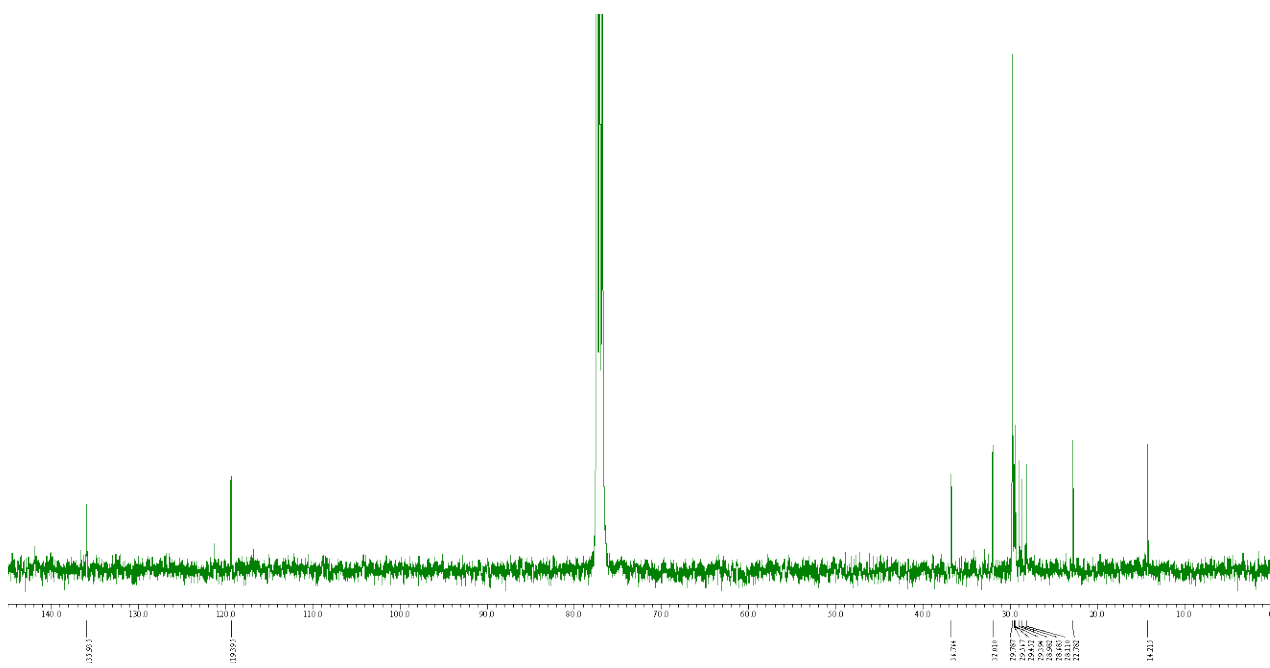
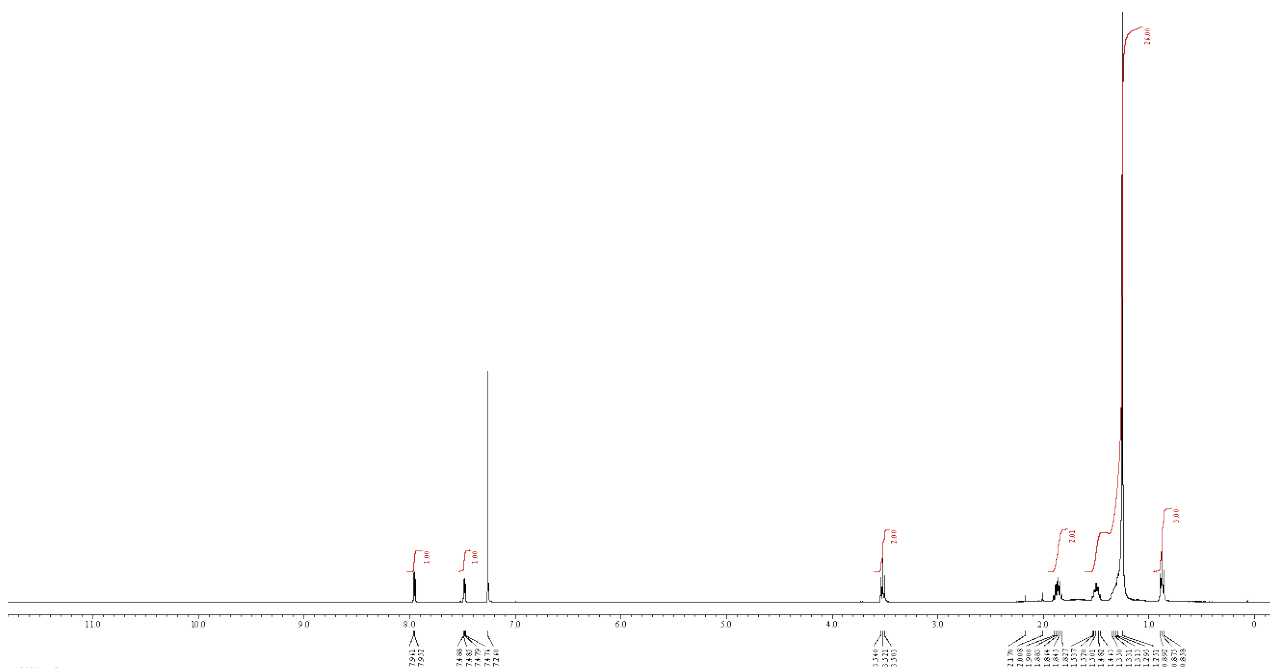
**3-18:0/stearyl bromide (molten)**



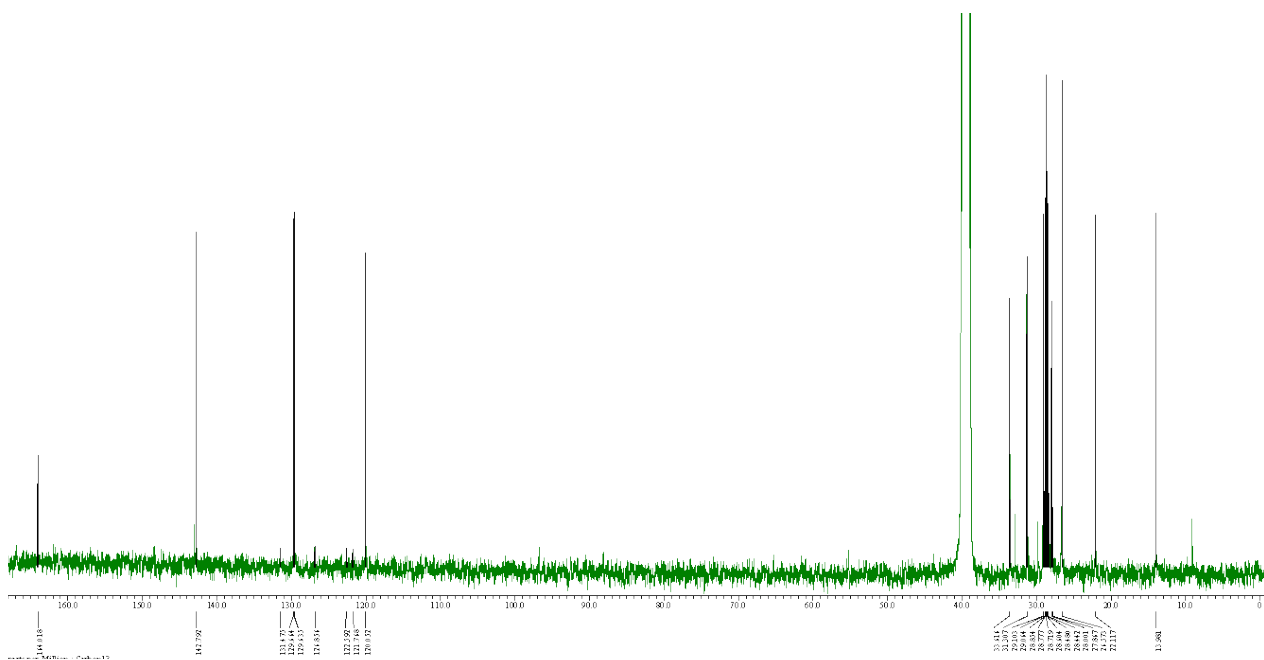
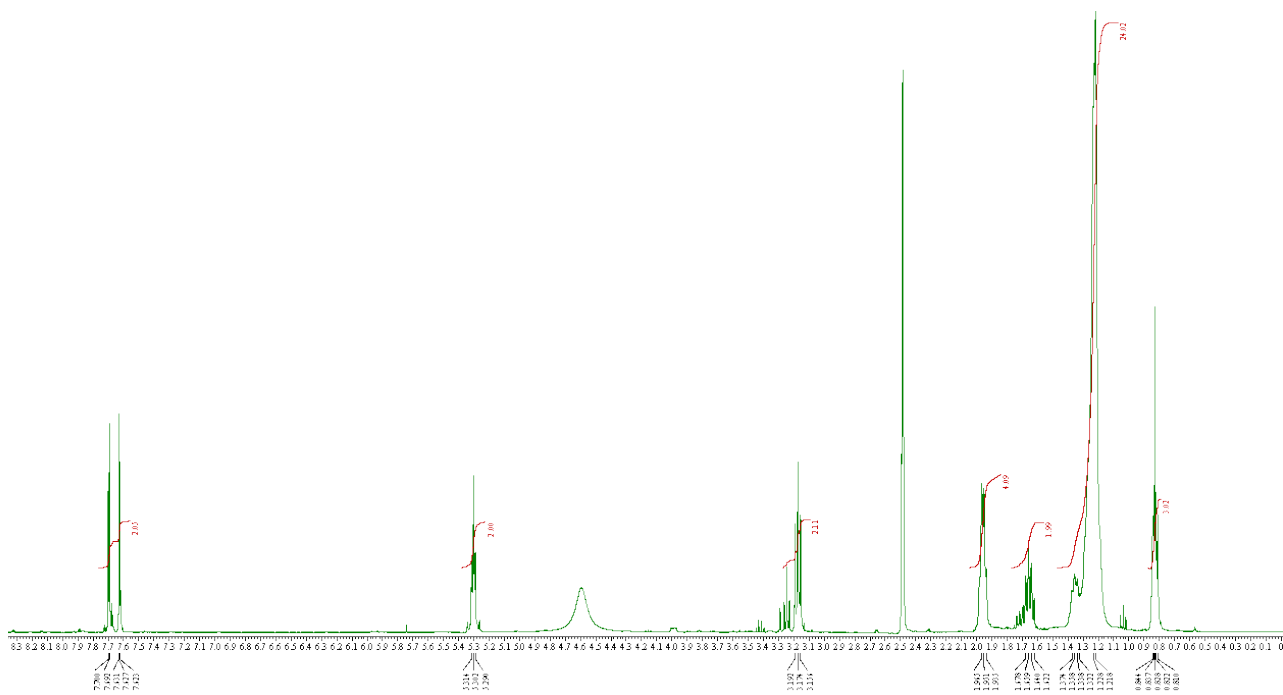


**<sup>1</sup>H and <sup>13</sup>C NMR spectra**

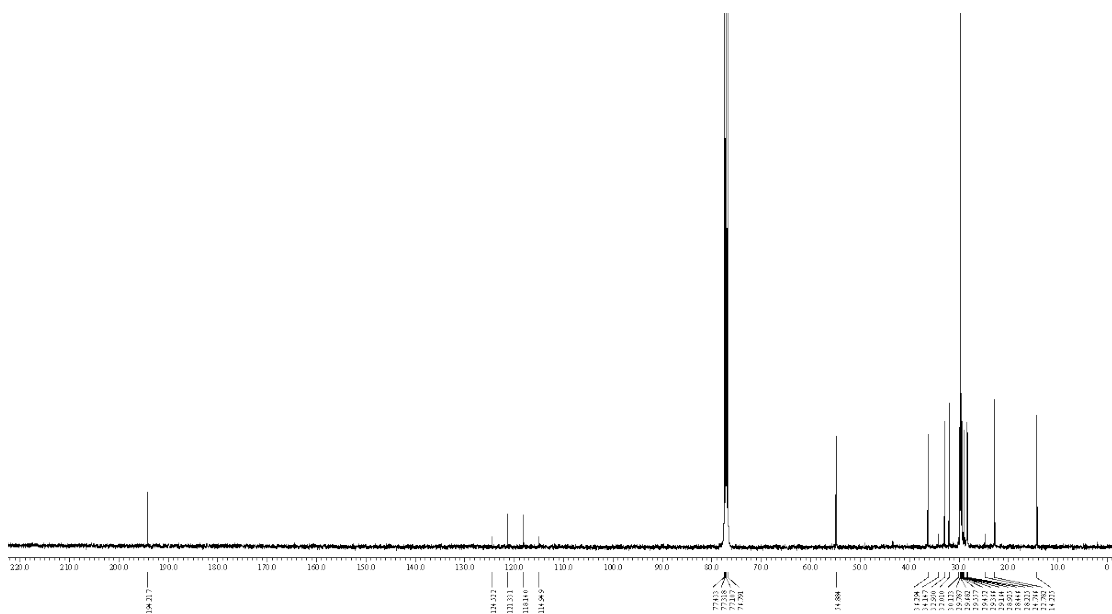
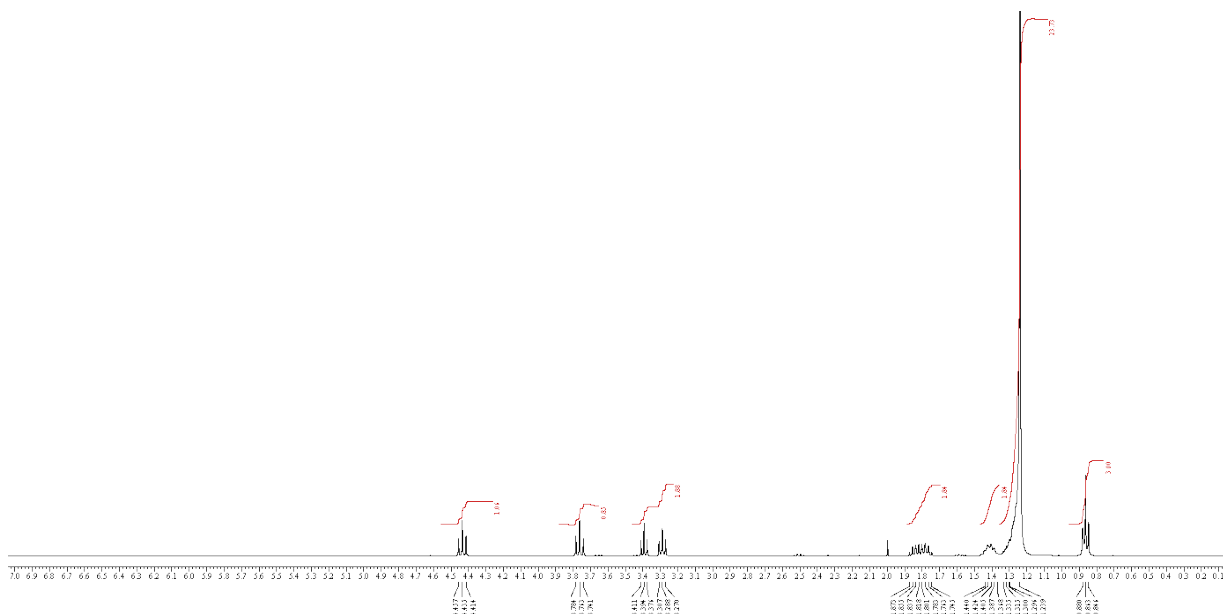
**3-16:0**



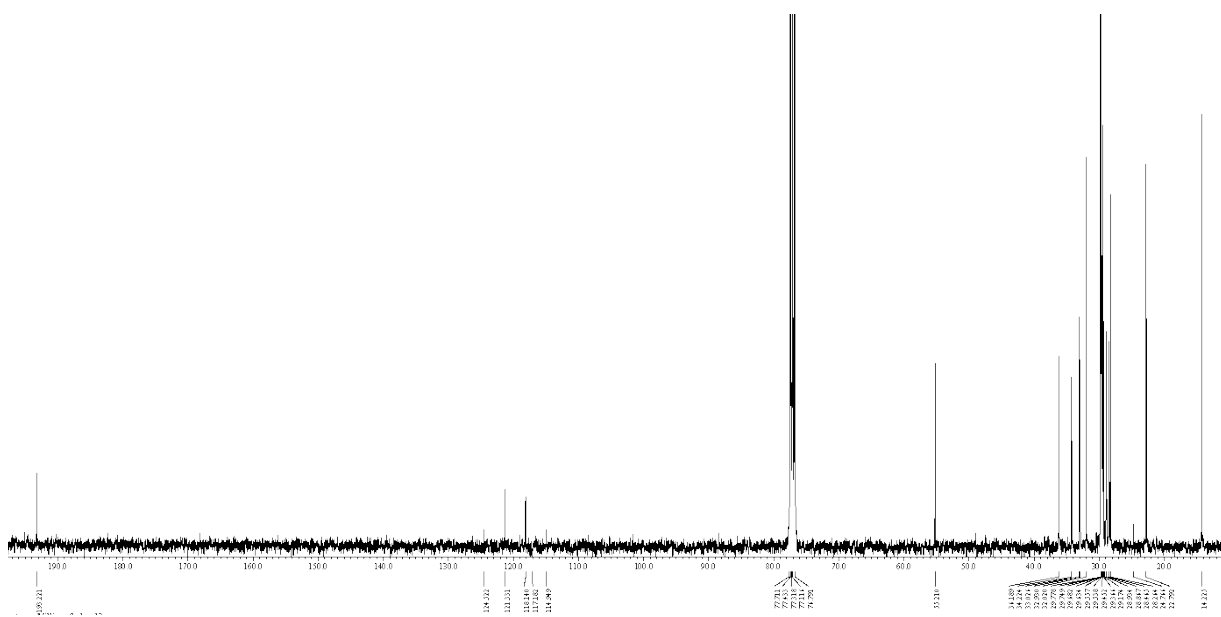
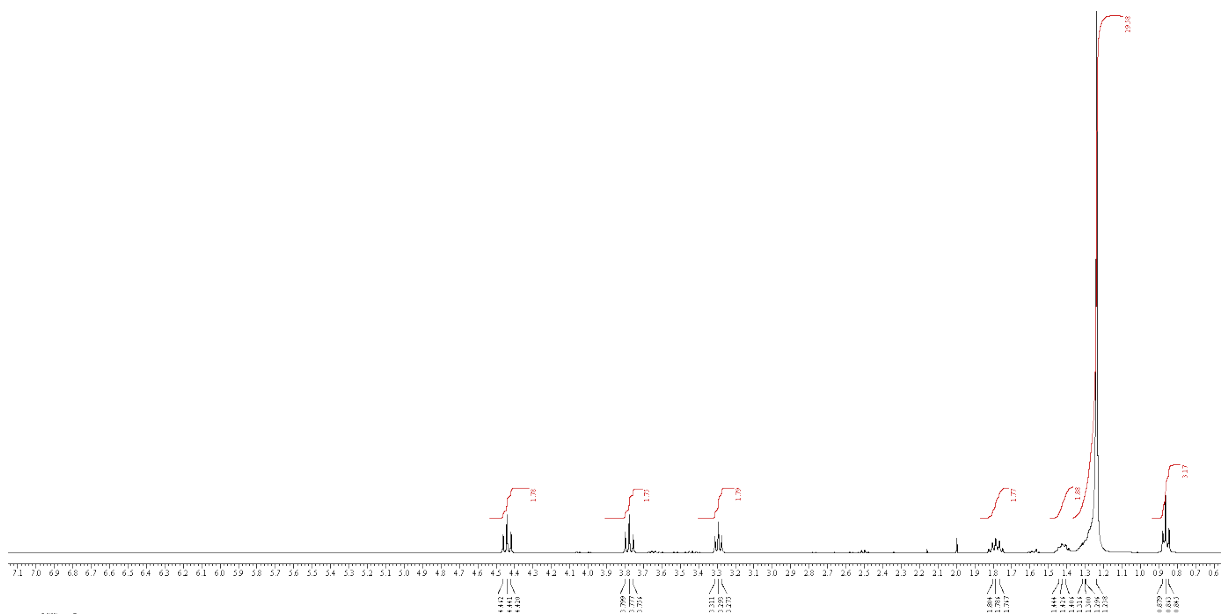




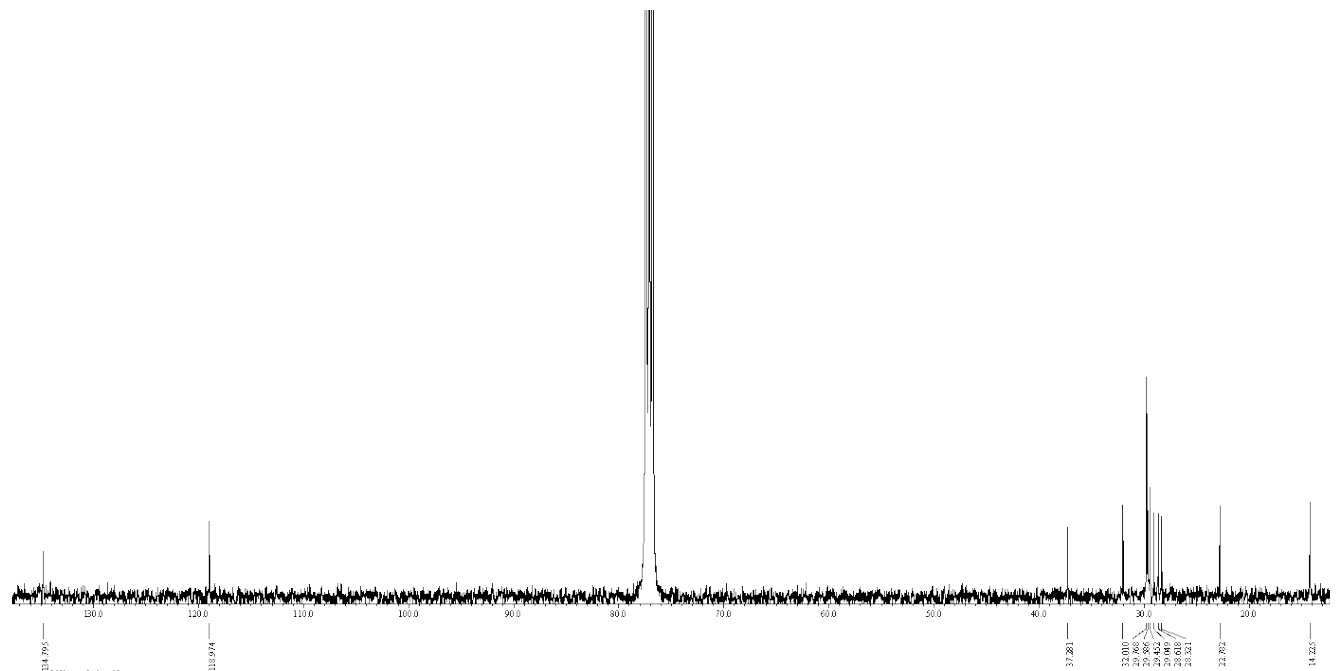
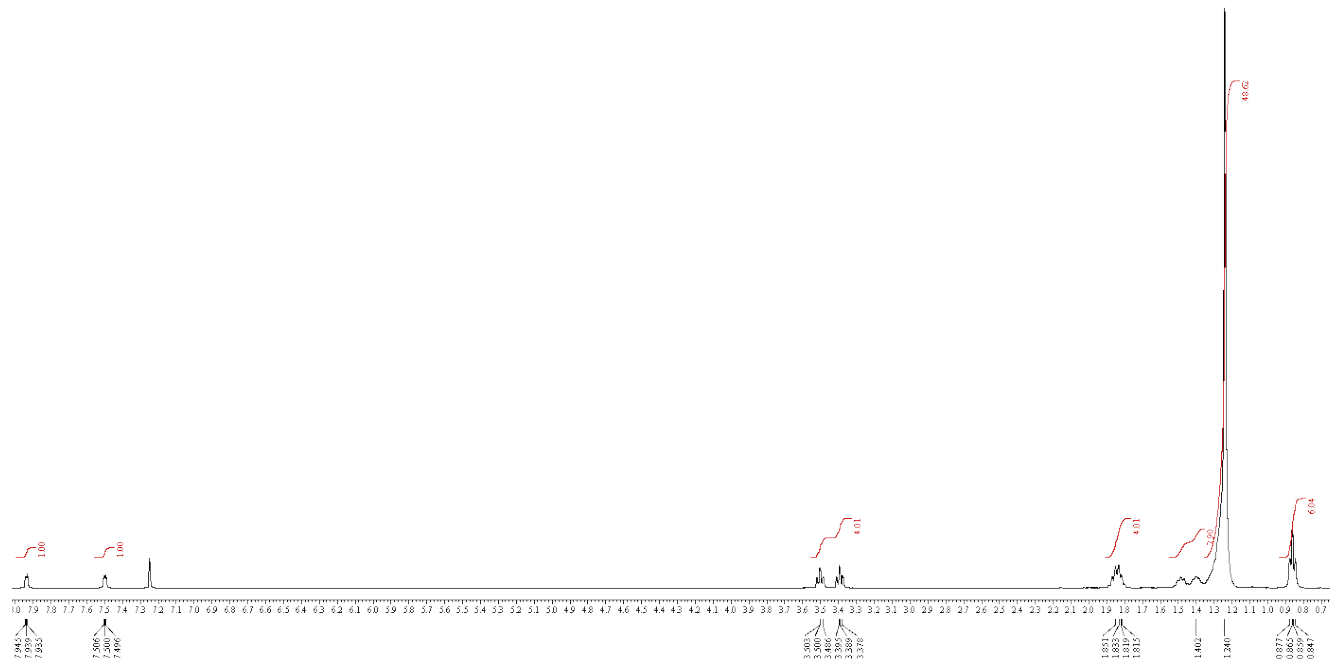
4-16:0



4-18:0



3-16:0/palmityl bromide (crystallized)



3-18:0/stearyl bromide (crystallized)

